The Evolving Scholar Vol. 3, 2023

https://dx.doi.org/10.59490/64fb0baca0066694c210e119

Bicycle and Motorcycle Dynamics 2023
Symposium on the Dynamics and Control of Single Track Vehicles
18–20 October 2023, Delft University of Technology, The Netherlands

Type of the Paper: Conference Paper

Modeling of a Bicycle Cargo Trailer with Magic Formula Tire Model for Vehicle Dynamics Simulation

Marius Miller[1,*], Markus Pfeil[1], Ralph Kennel[2], Raphael Murri[3]

[1] Department of Electrical Engineering, Ravensburg-Weingarten University of Applied Sciences (RWU), Germany; marius.miller@rwu.de, ORCID 0000-0002-4574-608X; markus.pfeil@rwu.de
[2] School of Engineering and Design, Technical University of Munich (TUM), Germany; ralph.kennel@tum.de
[3] School of Engineering and Computer Science, Bern University of Applied Sciences (BFH), Switzerland; raphael.murri@bfh.ch
[*] corresponding author

Name of Editor: Jason Moore
Submitted: 08/09/2023
Accepted: 21/09/2023
Published: dd/mm/yyyy

Citation: Miller, M., Pfeil, M., Kennel, R. & Murri, R. (2023). Modeling of a Bicycle Cargo Trailer with Magic Formula Tire Model for Vehicle Dynamics Simulation. The Evolving Scholar - BMD 2023, 5th Edition.

Abstract:

In modern and sustainable concepts for supply chains, cargo bicycles, and cargo trailers can be a target-oriented solution in urban areas. However, drivers should be aware of the dynamics of these systems since, in the case of a loaded trailer, the trailer mass significantly exceeds the mass of the towing vehicle. However, the electrification of cargo trailers opens up the possibility of equipping these systems with an intelligent control system. This type of control system can be based on a model or tested using a model of the system. For this reason, the present research presents a single-track model of a bicycle-trailer system that considers longitudinal dynamics as well. In addition, a detailed tire model of a typical tire for cargo bikes is integrated. With the help of a prototype trailer, which forms the basis for the model's parameters, measurement data is collected and compared with the simulation results. Within the scope of the comparison, speed, acceleration in longitudinal and lateral direction, hitch force, yaw rate, and the angle between the towing vehicle and trailer are compared in a longitudinal and lateral dynamic case. The presented model shows a good agreement with the reality in the longitudinal dynamic investigation regarding the tested scenarios. In terms of lateral dynamics, the model can reproduce a significant part of the measured data but exhibits minor differences related to environmental conditions, limited degrees of freedom, measurement errors, and the implementation of a needed driver model in this setup, which represents the human component. In the future, the model can be used to investigate the driving characteristics of bicycle-trailer systems. Furthermore, adding a model of the trailer powertrain and its control to the simulation can enable simulation-based design and testing of the required vehicle dynamics controller before implementation on a prototype.

Keywords: Cargo-trailer, Bicycle-trailer, Tire Modeling, Micromobility, Electrified Bicycle Trailer, Bicycle-trailer Model, Vehicle Dynamics

ISSN: 2667-2812

 https://dx.doi.org10.59490/64fb0baca0066694c210e119

1 Introduction

Electrically assisted cargo trailers allow the transportation of heavy loads using a sustainable towing vehicle such as a conventional bicycle. However, this results in configurations in which the towing vehicle, consisting of bicycle and driver, has a significantly lower weight than the loaded trailer. In certain situations, the trailer dynamics can critically affect the towing vehicle. This results in unstable and dangerous conditions such as jackknifing and swaying of the trailer. If an electrified trailer is used in a bicycle-trailer system, the trailer powertrain and an appropriate vehicle dynamics control can contribute to the overall safety. Since testing such a vehicle dynamics control system can be dangerous for the test driver, Miller et al. (2023b) suggests testing with the help of a simulation and, in a more advanced sense, with a hardware-in-the-loop (HIL) system. In this context, the simulation is based on a simplified model, which can include different levels of detail. The advantage of using a HIL system is that it enables the integration of the controller's target hardware to test if it is interacting with the developed software. Furthermore, other control units can be integrated as hardware to test if the systems interact as required. However, this test method is based on a reliable model that is consistent with the real-world application. The same applies to a model-based control strategy, whose quality is defined, among other things, by a model that fits the system. For this reason, a model with three degrees of freedom (3DOF) is presented in the context of the present investigations, which can be used to represent the vehicle dynamics of a trailer attached to a bicycle. The current model does not consider an electric powertrain of the trailer. This basic model can be used to investigate various driving dynamic situations to identify under which conditions the system becomes unstable and critical situations can arise regarding user safety. Based on these identified driving maneuvers, the evaluation of a vehicle dynamics controller can be performed. Existing studies, according to Korayem et al. (2022) point out the so-called "snaking" and "jack-knifing" as particularly critical situations in trailer systems. The phenomenon of "snaking" describes the swaying of the trailer due to lateral forces, especially on slippery surfaces. If a vehicle-trailer system is braked in a curve and the frictional force between the road and the tire is in saturation, the angle between the towing vehicle and the trailer can decrease significantly, resulting in a possible collision of the trailer with the towing vehicle, which is called "jack-knifing". In this context, Vempaty & He (2017) gives an overview of various approaches to stabilize tractor-trailer systems via the vehicle dynamics control of the tractor. Furthermore, the momentum of a fully loaded trailer can cause the comparatively light system of a bicycle and rider to be pushed by the trailer during braking.

The model of this research is based on the model presented by Korayem et al. (2022), but extended by a longitudinal dynamics model as can be seen in Miller et al. (2023b) and a detailed tire model. The tire model is based on a special tire for cargo bicycles measured and modeled according to Miller et al. (2023a), which is implemented as a magic formula (MF) model according to Pacejka & Besselink (2012).

The simulation results are then compared with the measured data of a prototype to evaluate whether the vehicle model corresponds to real-world conditions. Since there are no standardized test scenarios for driving dynamics testing of electrically powered bicycle trailers in Germany, two test scenarios are proposed to test the systems in simulation and in real-life testing. This involves comparing both a straight-ahead and an avoidance maneuver to allow the longitudinal and lateral behavior of the model to be evaluated. The trailer prototype used for comparison is a one-axle, all-wheel drive prototype with a system power of 2 kW. In addition to measuring acceleration and angular rates, a drawbar, according to Miller et al. (2021), enables direct measurement of the hitch force. In addition, an angle sensor is used to measure the angle between the bicycle and the trailer.

2 Modeling

Within the modeling framework, a mathematical description of the physical system behavior of the bicycle, rider, and trailer is carried out on a level that represents simplified real-world physical conditions. The bicycle-trailer model takes into account the forces acting on the system. The first part of the human driver is represented as a control system, which tries to follow a given speed trajectory by applying pedal force. The second part of the human driver is a predictive control system that tries to follow a given reference road trajectory by adjusting the steering angle. Modeling is carried out in Matlab SIMULINK. The vehicle model in the longitudinal and lateral direction is described first, followed by the tire model and concluding with the driver model.

ISSN: 2667-2812

https://dx.doi.org/10.59490/64fb0baca0066694c210e119

2.1 Vehicle Model

In the scope of the present investigations, a vehicle model is presented to analyze the yaw stability of bicycle-trailer systems in micromobility. The model shown in this research is a single-track model, which combines the trailer's axle on one track. Since the bicycle's wheels are already on one track, there is no simplification regarding the axles, as it is usually done when considering multi-track systems such as a car. According to He & Ren (2013), pitch and roll motions are of minor importance for these investigations and are therefore neglected when the analysis is performed with dual-track vehicles. In contrast, it must be noted that bicycles are driven not only by a steering angle but also by tilting the system. Because of this, a restriction compared to reality arises in this case since this degree of freedom is not available in the presented model. The analysis of this research will evaluate whether the proposed model can simulate the behavior of a bicycle-trailer system with a reduced set of degrees of freedom in a target-oriented way. Furthermore, the presented model does not consider the elevation of the road and is therefore only valid on even road surfaces. In addition to the lateral dynamics, the model also considers the longitudinal dynamic behavior of the system. A detailed description of the longitudinal model can be found in Miller et al. (2023b). A schematic representation of the presented single-track model can be found in Figure 1.

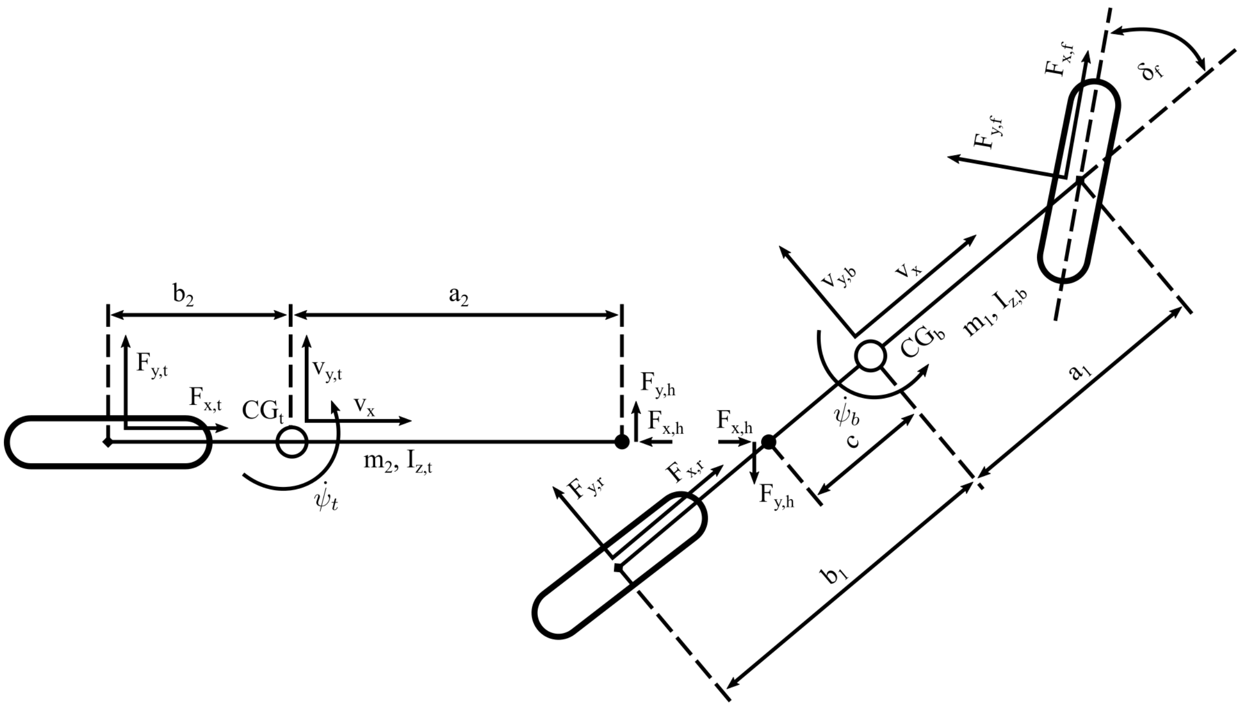

Figure 1. Bicycle Trailer Systems as a single track model.

As can be seen in Figure 1, the two subsystems consisting of bicycle and trailer can be coupled to each other via the hitch forces $F_{x,h}$ and $F_{y,h}$ acting in the x and y directions at the hitch. The resulting Equations of motion are given by Equation 1 to 4:

$$m_b(\dot{v}_{y,b} + v_x\dot{\psi}_b) = F_{y,f} + F_{y,r} - F_{y,h} \tag{1}$$

$$I_{z,b}\ddot{\psi}_b = a_1F_{y,f} - b_1F_{y,r} + cF_{y,h} \tag{2}$$

$$m_t(\dot{v}_{y,t} + v_x\dot{\psi}_t) = F_{y,t} + F_{y,h} \tag{3}$$

$$I_{z,t}\ddot{\psi}_t = -b_2F_{y,t} + a_2F_{y,h} \tag{4}$$

The forces $F_{y,f}$, $F_{y,r}$, and $F_{y,t}$ acting on the tire are no constant forces but describe complex interactions of the tire with the road. In the context of the presented work, these are modeled as a function of the respective slip angle of the wheel and its contact force F_z. This model will be explained in more detail in the subsequent section.

ISSN: 2667-2812

https://dx.doi.org/10.59490/64fb0baca0066694c210e119

2.2 Tire Model

The tire behavior of the bicycle and trailer is modeled using a generic form of the Magic Formula (MF) model according to Pacejka & Besselink (2012) and the results of Miller et al. (2023a). This model considers the tire characteristics in the longitudinal and lateral direction as a function of the slip κ as well as the slip angle α of the wheel and the contact force, but under the assumption that no camber angles occur. Regarding the tire model, it is assumed that bicycle and trailer use 20 in wheels with the tires described in Miller et al. (2023a). While this is true for the trailer with one axle and two wheels when operated on an even surface, a bicycle can be driven with camber angles $\neq 0°$. At this point, the modeling differs from reality, as the presented three degrees of freedom (3DOF) model allows for motion in the xy plane as well as rotation about the z-axis but does not allow for rotation of the system around the x- or y-axis. In this research, the measured tire data from Miller et al. (2023a) is normalized using the F_z force. Afterwards, the coefficients of the generic MF are optimized using the non-linear least squares method so that the mathematical model fits the measured data as accurately as possible. The model generated this way becomes a function of κ or α and the vertical force F_z as described in Equation 5 and 6.

$$F_{x,i}(\kappa_i, F_z) = F_z((Dsin(Carctan(B\kappa_i - E(B\kappa_i - arctan(B\kappa_i)))))) \tag{5}$$

$$F_{y,i}(\alpha_i, F_z) = F_z((Dsin(Carctan(B\alpha_i - E(B\alpha_i - arctan(B\alpha_i)))))) \tag{6}$$

Where i represents the index for each tire position since the slip angles can differ from the respective axle and tire positions. The coefficients of the MF model determined by optimization are listed in Table 1 with the respective goodness of fit. The resulting tire models are visualized in figure 2.

Table 1. Parameters - Normalized MF tire model.

	Value	SSE	R^2
B_x	0.1803	8.612	0.9807
C_x	1.469		
D_x	1.114		
E_x	0.7769		
B_y	0.1826	10.25	0.9944
C_y	1.533		
D_y	1.289		
E_y	0.7658		

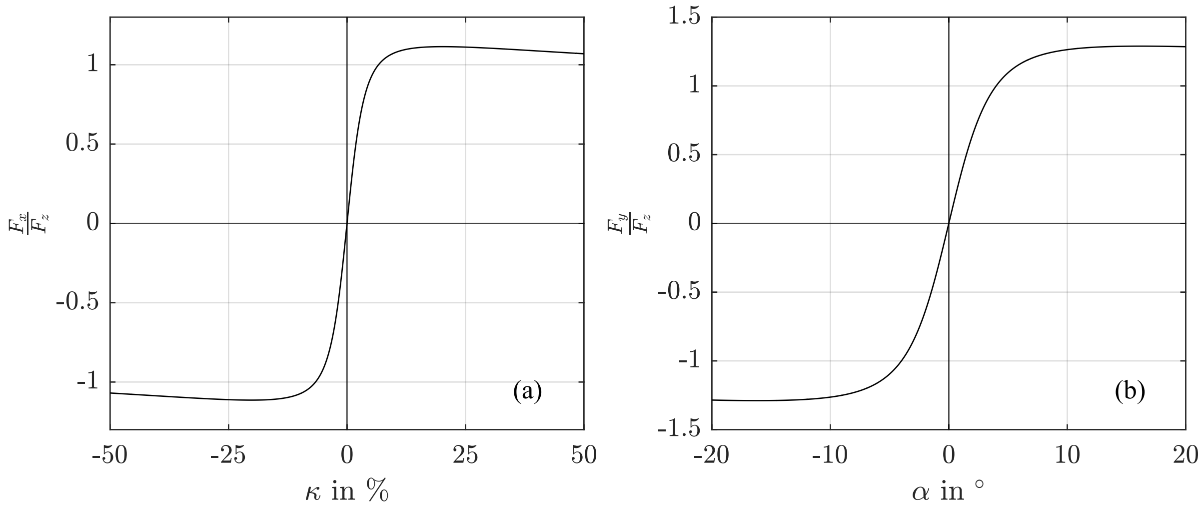

Figure 2. Normalized MF tire model of a Schwalbe Pick-Up 20 × 2.15 in tire at p = 3.5 bar where (a) shows the $F_x(\kappa)$ and (b) shows the $F_y(\alpha)$ relation.

ISSN: 2667-2812

 https://dx.doi.org/10.59490/64fb0baca0066694c210e119

In order to represent the lateral dynamics of the system, the respective slip angles of the associated wheels are required. According to Chen & Tomizuka (1995), the slip angles at the front, rear, and trailer axles are defined by Equations 7 to 9.

$$\alpha_f = \delta_f - arctan\left(\frac{v_{y,b} + a_1\dot{\psi}_b}{v_x}\right) \tag{7}$$

$$\alpha_r = -arctan\left(\frac{v_{y,b} - b_1\dot{\psi}_b}{v_x}\right) \tag{8}$$

$$\alpha_t = -arctan\left(\frac{(v_{y,t} - c\dot{\psi}_b)cos(\psi_b - \psi_t) - \dot{\psi}_t(a_2 + b_2) + v_x sin(\psi_b - \psi_t)}{v_x cos(\psi_b - \psi_t) - (v_y - c\dot{\psi}_b)sin(\psi_b - \psi_t)}\right) \tag{9}$$

2.3 Driver Model

A driver model is required to drive and steer the vehicle model. The implementation follows the two control loops shown in Figure 3. A PI controller is used in the model to track a given velocity reference trajectory. The error is calculated by comparing the given reference velocity v_{ref} with the current longitudinal velocity v_x with respect to the body coordinate system of the towing vehicle. The proportional term of the PI controller multiplies the current error by a gain factor K_p. The second part of the PI controller consists of an integral term, which includes the time integration of the error and multiplies this part by the factor K_i. Normalization over the nominal velocity v_{nom} results in an output quantity of the system between zero and one as t_{gain}. This percentage output of the controller is then multiplied by a simulated maximum available driver torque. In an initial driver simulation, the results according to Korff et al. (2007) were adopted simplistically, resulting in a torque T_c at the crank by the driver of approx. 40 Nm, which is not constant but dependent on the position of the crank. For this reason, the torque curve is superimposed with an ideal sine to represent the described behavior in a simplified form. The frequency of the sine wave is 2.1 Hz, which results from the obtained cadence during the test drives. To avoid numerical problems, the superimposed sine wave is only applied at speed values higher than $2.5\frac{m}{s}$. In addition, high torques of up to 100 Nm are temporarily permitted for start-up, which can occur in real-world operation by standing pedal operation. The resulting torque is transferred to the bicycle-trailer system, where the movement is computed.

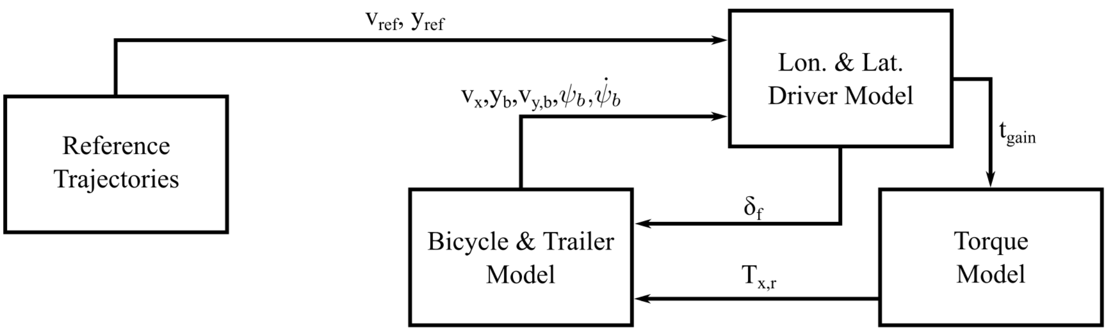

Figure 3. Driver Model.

The steering controller is implemented according to MacAdam (1988). This second predictive controller tries to follow a given y_{ref} trajectory by using a built-in bicycle model of the system. The controller needs v_x, y_b, $v_{y,b}$, ψ_b and $\dot{\psi}_b$ as feedback values and computes the front wheel steering angle δ_f as an output for the bicycle and trailer system, which computes the lateral movement of the system. According to MacAdam (1988), the driver behavior can be adjusted by the response time of the driver τ_{resp} and the prediction horizon P. The parameters for the driver model can be seen in Table 2. While the PI-controller parameters are adjusted by minimizing the error between v_{ref} and v_x, the lateral controller's parameter τ_{resp} was chosen with 0.4 s corresponding to a medium reaction time to an unintended collision avoidance maneuver. With a value of 0.35 m, the preview distance P has a small value, so an unforeseen avoidance maneuver is suggested to the simulated driver. A small preview distance corresponds to the real-world measurements since small traffic cones were used, which led to late recognition of the evasion point. It is important to note that a

ISSN: 2667-2812

https://dx.doi.org/10.59490/64fb0baca0066694c210e119

Table 2. Parameters for Driver Model.

Area	Parameter	Value
Longitudinal	K_p	13
Longitudinal	K_i	5
Longitudinal	v_{nom}	5
Lateral	τ_{resp}	0.4
Lateral	P	0.35

general replication of human driver behavior remains challenging since each driver has their own characteristics when it comes to accelerating, braking, and steering. Therefore, the presented parameters form a model of one driver type.

3 Prototype Trailer and Measurement System

The prototype trailer is a single-axle system with a wheel hub motor on each side. The main frame is made of aluminum profiles and offers cargo storage up to a length of 1.40 m and a width of 0.81 m. The trailer's hitch is placed in the center and attached to the bicycle with the help of a ball hitch. The values of the masses, mass inertias, drag coefficients, as well as the areas and dimensions of the trailer and an exemplary bicycle are listed in Table 3. For subsequent control of the trailer, the system has sensors, a central

Table 3. Parameters for Simulation.

Parameter	Value	Unit	Description
m_b	100.00	kg	Bicycle + Driver
$I_{z,b}$	3.73	kgm^2	Moore et al. (2009)
$c_{d,b}$	1.10		Chowdhury & Alam (2012)
$A_{f,b}$	0.50	m^2	Chowdhury & Alam (2012)
a_1	0.57	m	From CAD Model
b_1	0.41	m	From CAD Model
c	0.17	m	From CAD Model
m_t	112.60	kg	From CAD Model
$I_{z,t}$	45.17	kgm^2	From CAD Model
$c_{d,t}$	1.10		Chowdhury & Alam (2012)
$A_{f,t}$	0.85	m^2	From CAD Model
a_2	1.91	m	From CAD Model
b_2	0.13	m	From CAD Model

vehicle dynamics control unit (VDCU), and an electric powertrain, which are visualized in the system layout in Figure 4. The powertrain consists of a 48V battery with 29.7Ah and two VESC 6 75 power electronics, which drive two 1kW wheel hub motors via field-oriented control using software developed by Vedder (2023). With the help of a DC/DC converter, all sensors, including the VDCU, are supplied with voltage. The sensorset includes the sensors listed in Table 4. In addition to the standard methods of

Table 4. Sensorset of prototype trailer.

Sensor	Measured Value(s)	Communication	Description
Load Cells	hitch force $F_{h,x}$	Analog Signal	BCM 169H
Hitch Angle Sensor	hitch angle θ	Analog Signal	Novotechnik RFD-4021
IMU	acceleration $\dot{v}_x$, $\dot{v}_y$ and yaw rate $\dot{\psi}_z$	CAN-Bus	Movella / Xsens MTi-630
Power Electronics	wheel speed right rpm_r, wheel speed left rpm_l and respectively v_r and v_l measurement	CAN-Bus	TRAMPA BOARDS VESC 6 75V

measuring speeds and accelerations, the trailer has a system for measuring the hitch force according to Miller et al. (2021), which is based on load cells. Furthermore, an angle sensor is used to measure the hitch angle between the trailer and the towing vehicle. The values of the sensor are sampled by the VDCU with 80 Hz. While the power electronics and the inertial measurement unit (IMU) communicate via CAN-Bus, the load cells and hitch angle sensor signals are analog signals processed directly by the VDCU.

ISSN: 2667-2812

 https://dx.doi.org10.59490/64fb0baca0066694c210e119

For post-processing and analysis of the measured data, a CAN-Bus logger is included in the system, which gets time synchronized values from the VDCU. The control of the power electronics is done via CAN-Bus by the VDCU, which is not used in the present investigations to ensure that both model and simulation are compared in the same setup without additional torque of the electric drives.

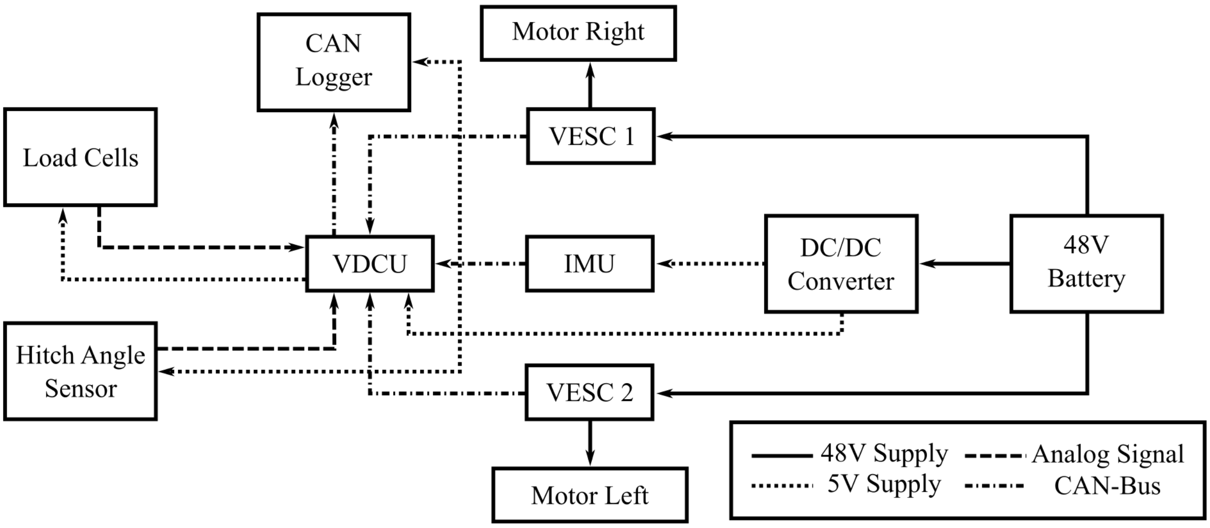

Figure 4. System layout - Prototype trailer.

The trailer prototype with the described measurement system attached to a bicycle is shown in Figure 5.

Figure 5. Prototype trailer attached to a bicycle.

4 Test Cases

A comparative analysis with measurement data from test drives with the prototype is carried out to evaluate the model presented in this paper. Within the scope of these tests, both the longitudinal and the lateral dynamic behavior are to be evaluated. For this reason,

ISSN: 2667-2812

a straight-line drive without steering intervention by the driver (longitudinal test case) and an avoidance maneuver (lateral test case) is performed with the prototype trailer and in the simulation. Regarding the longitudinal test case, acceleration is performed from 0 $\frac{m}{s}$ until a final speed of approx. 4 $\frac{m}{s}$ is reached. After a short constant travel of 4 $\frac{m}{s}$, a braking maneuver is performed until the vehicle comes down to a velocity of 0 $\frac{m}{s}$ again. The lateral test case also starts from 0 $\frac{m}{s}$, after acceleration up to a speed of approx. 4 $\frac{m}{s}$, the speed is kept constant for a short section before the collision avoidance is performed. The obstacle to avoid has a lateral length of 1.5 m and is placed at a 1 m distance to the evasion point, resulting in a situation that should replicate an unexpected maneuver. Afterwards, the system is decelerated to 0 $\frac{m}{s}$ again.

5 Comparison of Measured and Simulated Data

In the first investigation, the longitudinal dynamic characteristics of the model are compared with the measured data. In this context, the velocity v_x and the acceleration $\dot{v}_x$ in the vehicle-fixed coordinate system as well as the measured hitch force $F_{x,h}$ in the drawbar are compared with each other. Figure 6 shows the measured and simulated data for the longitudinal test case. The indices "meas" represents data obtained with the prototype, while "sim" shows data generated during simulation with the presented model. The reference speed $v_{x,ref}$ as input for the driver model results from an average value of the left $v_{x,l,meas}$ and right $v_{x,r,meas}$ wheel speed, which was measured during the test drive.

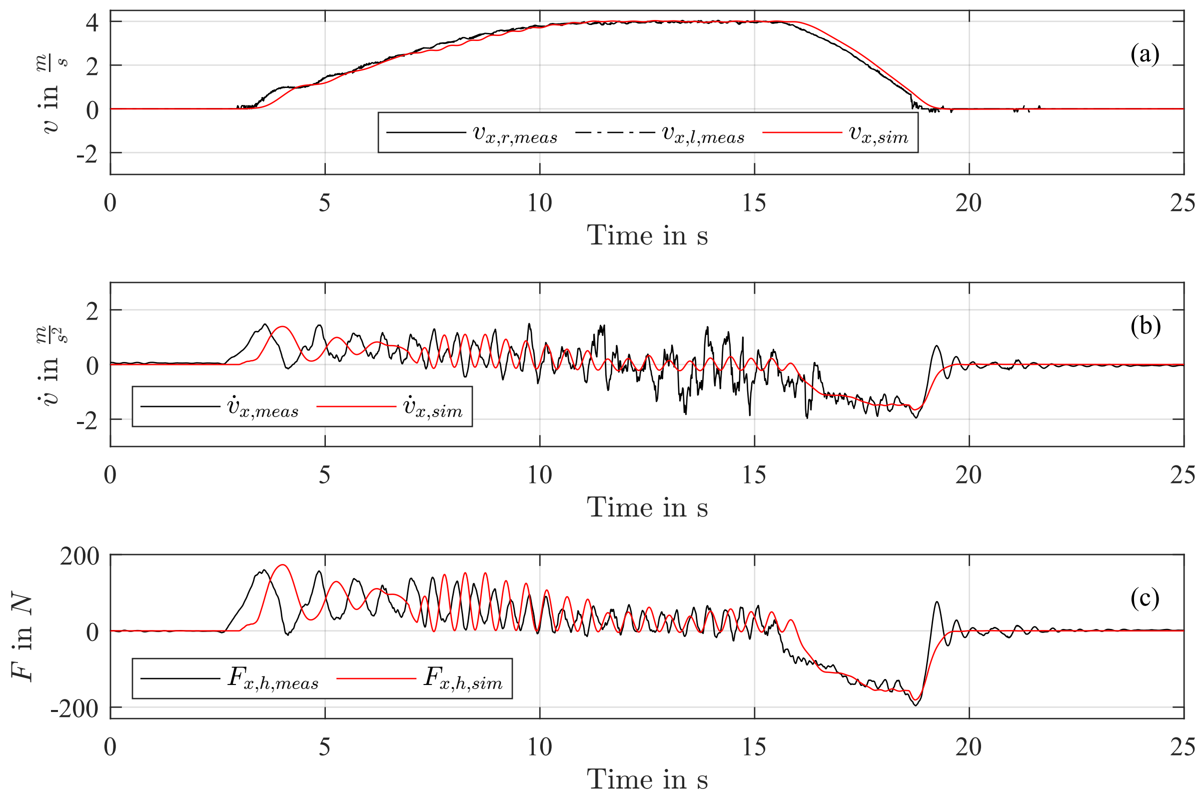

Figure 6. Longitudinal test case - Comparison of measured data and simulation results where (a) shows the velocity v_x, (b) shows the acceleration $\dot{v}_x$ and (c) shows the hitch force $F_{x,h}$.

As can be seen in Figure 6 (a), the simulated bicycle tries to follow the reference v_x signal given by the measured data. With a short delay of approx. 0.25 s, the model achieves to meet the required speed of approx. 4 $\frac{m}{s}$. The sinusoidal amplitudes of the $\dot{v}_{x,meas}$ signal result from the periodic torque output at the cyclist's crank. Despite sinusoidal modeling of the torque, the model's $\dot{v}_{x,sim}$ signal does not exactly reproduce the peaks of the acceleration amplitudes of the measured signal. One reason for this is the threshold value of $2.5\frac{m}{s}$, which must be exceeded for the model to perform a sinusoidal torque superposition. Moreover, the pedal frequency of a cyclist varies depending on the situation, which cannot be represented by a fixed superposition frequency as used

ISSN: 2667-2812

 https://dx.doi.org/10.59490/64fb0baca0066694c210e119

in the model. However, it is evident in the time domain that the frequencies of the sinusoidal waves of both systems are similar but show a phase shift. High similarity regarding the amplitudes can be seen by comparing $F_{x,h}$ of the model and measured data, whereas the simulated data exhibits the described lack of 0.25 s. During acceleration, a positive peak of 160.26 N is obtained in $F_{x,h,meas}$, which the model almost exactly meets with a value of 173.41 N. The same behavior can be seen during deceleration, where a negative peak of -196.32 N is obtained in $F_{x,h,meas}$. Whereas the simulation reaches a value of -181.05 N for $F_{x,h,sim}$, resulting in a difference of 15.27 N. In the second investigation, the lateral test case is compared. Figure 7 shows the measured and simulated data for the lateral test case.

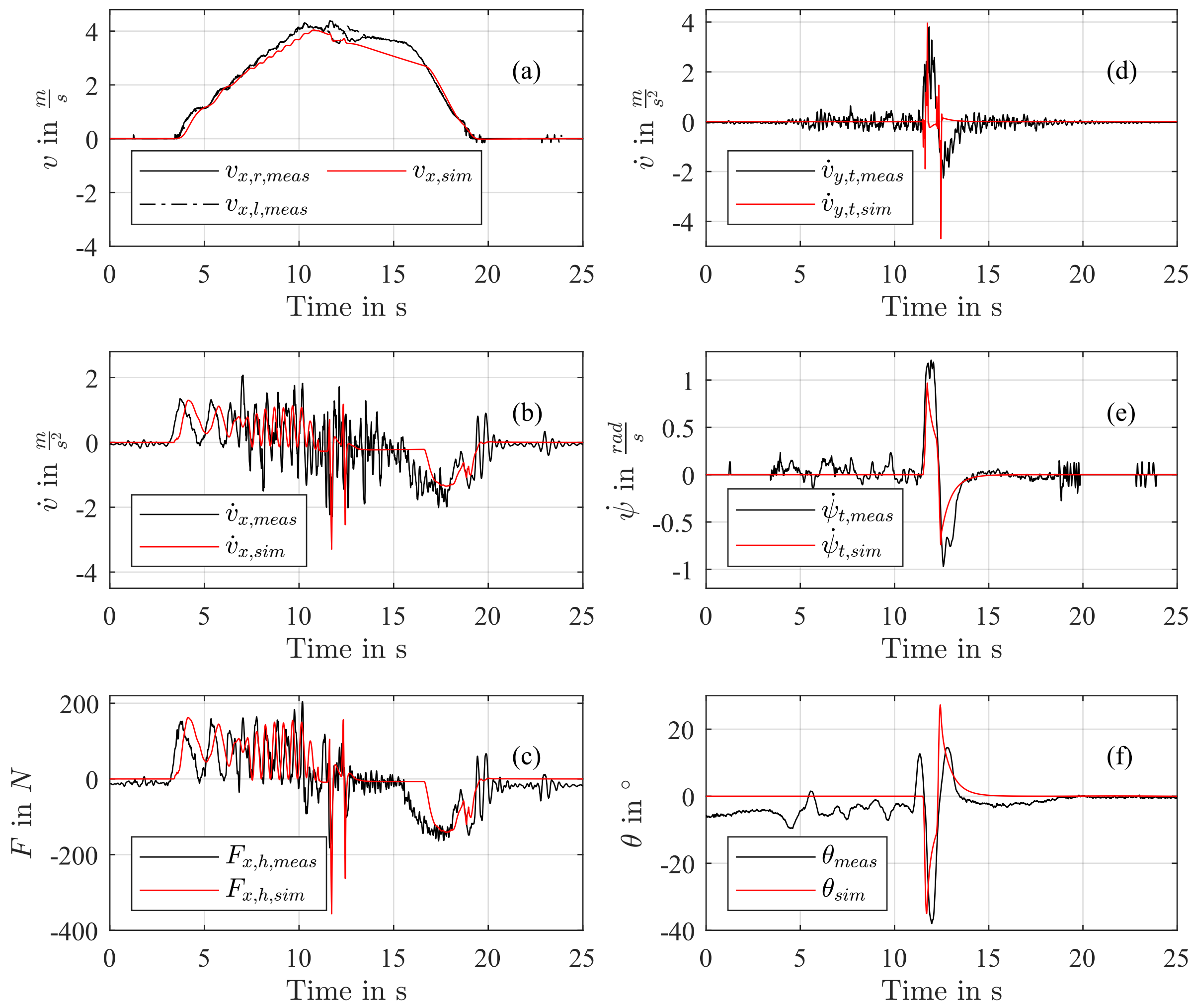

Figure 7. Lateral test case - Comparison of measured data and simulation results where (a) shows the velocity v_x, (b) shows the acceleration $\dot{v}_x$, (c) shows the hitch force $F_{x,h}$, (d) shows the acceleration $\dot{v}_y$, (e) shows the yaw rate $\dot{\psi}_t$ and (f) shows the hitch angle θ.

As in the longitudinal dynamic test case, the longitudinal velocity of the measured data is used as $v_{x,ref}$ signal for the simulation. The model's controller tracks the model's speed v_x and adjusts the torque so the given $v_{x,ref}$ curve can be followed with a slight delay. The periodic torque output, caused in real-world measurements by pedaling, can be seen in the $\dot{v}_x$ signal of the measured data during acceleration as a sinusoidal superposition of the signal. The simulation, which has a fixed simulated pedaling cadence, can reproduce this behavior to some extent, as can be seen from approx. 7.5 s to 11 s. The acceleration peaks occurring in this case are slightly higher in the measured data. During the real-world test, there was no active braking during the avoidance maneuver and no pedaling after the avoidance maneuver. For this reason, braking is only allowed for $t > 15\ s$, and pedaling is prevented in the simulation for $t > 15\ s$. As a result, the $\dot{v}_{x,sim}$ curve shows only a slightly negative signal in this period due to the speed falling

ISSN: 2667-2812

 https://dx.doi.org/10.59490/64fb0baca0066694c210e119

from the driving resistances. As can be seen in Figure 7 (a), braking is initiated from 16.7 s, which can be seen in Figure 7 (c) with a pushing trailer and negative hitch force values in $F_{x,h,meas}$. The simulated signal $F_{x,h,sim}$ also shows this decrease and results in a negative peak value of -141.20 N, while $F_{x,h,meas}$ has a negative peak of -163.72 N. The resulting difference is therefore given as an absolute value of 22.52 N. From 11.25 s the avoidance maneuver takes place, which can be seen in the measurement data via a positive and a negative deflection in the signals of $\dot{v}_{y,t}$ and $\dot{\psi}_t$ in Figure 7 (d) and (e). The positive amplitude of $\dot{v}_{y,t,meas}$ with 3.81 $\frac{m}{s^2}$ is closely met by $\dot{v}_{y,t,sim}$ with a value of 3.96 $\frac{m}{s^2}$. Regarding the negative amplitude of $\dot{v}_{y,t,meas}$ with -2.26 $\frac{m}{s^2}$, the simulation is reaching a value of -4.69 $\frac{m}{s^2}$. For this purpose, it is assumed that the filter profile of the IMU leads to an attenuation of the measured amplitude so that the true value could be higher and closer to the simulation. The investigation of this assumption will be examined in the context of new measurements so that the deviation of the negative amplitude can be evaluated. Further, it must be mentioned that the measurements of the test drives were carried out on a concrete surface. The tire measurements, which serve to create the tire model, were carried out on asphalt. The resulting different slip values also influence the behavior of $\dot{v}_{y,t,meas}$. Regarding the angular velocity, shown in Figure 7 (e), it can be seen that the model can reproduce the data of the real test run with a small error. The positive peak of the measured data is at 1.18 $\frac{rad}{s}$, while the model shows a nearly identical maximum with 0.97 $\frac{rad}{s}$. The negative peak of the real data with -0.97 $\frac{rad}{s}$ can be reproduced by the model as well with -0.74 $\frac{rad}{s}$. In comparison with $\dot{\psi}_{t,meas}$, the shape of $\dot{\psi}_{t,sim}$ is more edged, which is caused by the steering characteristics of the simulated driver. Looking at θ in Fig. 7 (f), it is recognizable that the simulation data follows the measured data with a good fit after 10 s. With a peak of -34.99 °, θ_{sim} has a peak of almost the same size as θ_{meas}, which has a value of 37.98 °. The difference up to the time of 10 s results from a not exactly in-one-line standing trailer and bicycle at the start of the test drive. This offset improves in the course of approx. 15 s and settles at approx. -0.2 °, which results from the measurement inaccuracy of the sensor and the positioning error of the sensor on the bicycle.

6 Conclusion

In the present work, the modeling of a bicycle trailer was investigated using a single-track model with an additional longitudinal dynamics model. The model includes a nonlinear tire model based on the not linearized calculations of the slip angles. The normalized tire model is built on the research of Miller et al. (2023a) and is used in a lateral vehicle dynamics simulation for the first time. A combined driver model based on a longitudinal and lateral controller has been introduced to follow a reference longitudinal velocity and a lateral trajectory. With the help of a new trailer prototype, test drives were performed, and measurement data was collected. In the case of validating the proposed vehicle model, the measured data was compared to the simulation results. In this context, the measured velocity of the prototype and a defined test scenario serve as inputs for the simulation. While the longitudinal dynamics model shows a good alignment between simulated and measured data, there is a slight deviation in the model compared to reality in the context of lateral dynamics. Regarding this relation, the model's driver has a significant impact, as the steering angle and the shape of the steering input affect the overall system's behavior. The parameters of the driver controller have a corresponding weighting when comparing simulation data with measured data. Mapping the human behavior in this framework is one of the major difficulties, as no steering signal was measured from the cyclist. Furthermore, the present tests were performed on a concrete surface, while the data for the tire model was measured on asphalt. Different friction values between the model and the real-world scenario can lead to varying values of the slip angle α, resulting in deviations of the lateral acceleration $\dot{v}_y$. On the other hand, measurement error can also lead to an error between the simulated and measured signals. Regarding this topic, the settings of the IMU can lead to deviations as well. The IMU is assumed to be responsible for the damping of occurring acceleration peaks by its internal filters. Despite the mentioned deviations, the presented model shows a target-oriented fit since rotating movements around the x- and y-axis, especially with the towing vehicle, are not considered in the model. Thus, the presented model can be used to investigate vehicle dynamic stability. Furthermore, the model can be supplemented by a powertrain simulation as presented in Miller et al. (2023b), allowing the control of an electrically driven trailer to be tested, for example, with a hardware-in-the-loop system before implementation on a prototype.

References

Bechtloff, J. (2017). *Schätzung des Schwimmwinkels und fahrdynamischer Parameter zur Verbesserung modellbasierter Fahrdynamikregelungen*. Technische Universität Darmstadt

Chen, C., Tomizuka, M. (1995), Dynamic Modeling of Tractor-Semitrailer Vehicles in Automated Highway Systems. California PATH Working Paper, UCB-ITS-PWP-95-8.

ISSN: 2667-2812

Chowdhury, H., Alam, F. (2012), Bicycle aerodynamics: an experimental evaluation methodology. Sports Eng (2012), 15. DOI 10.1007/s12283-012-0090-y

He, Y. and Ren, J. (2013), A Comparative Study of Car-Trailer Dynamics Models. In SAE Int. J. Passeng. Cars - Mech. Syst. 6(1):177-186, https://doi.org/10.4271/2013-01-0695

Kiencke, U., Nielsen, L. (2005) *Automotive Control Systems - For Engine, Driveline, and Vehicle*,. 2nd ed.; Springer Berlin: Heidelberg, Germany.

Korayem, A.H., Khajepour, A., Fidan B. (2022), A Review on Vehicle-Trailer State and Parameter Estimation. In IEEE Transactions on Intelligent Transportation Systems, vol. 23, no. 7, pp. 5993-6010, July 2022, doi: 10.1109/TITS.2021.3074457

Korff, T., Romer, L. M., Mayhew, I.; Martin, J. C. (2007), Effect of Pedaling Technique on Mechanical Effectiveness and Efficiency in Cyclists. Medicine & Science in Sports & Exercise 39(6):p 991-995, June 2007. DOI: 10.1249/mss.0b013e318043a235

MacAdam, C. C. (1988), Development of Driver/Vehicle Steering Interaction Models for Dynamic Analysis. Final Technical Report UMTRI-88-53. Ann Arbor, Michigan: The University of Michigan Transportation Research Institute.

Miller, M., Kaufmann, A., Reick, B., & Pfeil, M. (2021), Intelligente Anhängerdeichsel für verschiedene Zugfahrzeuge. Hochschule Ravensburg-Weingarten, Weingarten

Miller, M., Pfeil, M., Reick, B., Murri, R., Stetter, R., & Kennel, R. (2023a), Measurement and Modeling of a Cargo Bicycle Tire for Vehicle Dynamics Simulation. Applied Sciences, 13(4), 2542. https://doi.org/10.3390/app13042542

Miller, M., Pfeil, M., & Kennel, R. (2023b), Trailer Electrification–A HIL Approach for MPC Powertrain Control to Ensure Driver Safety in Micromobility (No. 2023-24-0180). SAE Technical Paper, doi:10.4271/2023-24-0180

Moore, J., Kooijman, J., Hubbard, M. & Schwab, A. (2009), A Method For Estimating Physical Properties of a Combined Bicycle and Rider, *Proceedings of the ASME 2009 International Design Engineering Technical Conferences & Computers and Information in Engineering Conference IDETC/CIE 2009*, San Diego, California, USA

Pacejka, H.B., Besselink, I. (2012) *Tire and Vehicle Dynamics*, 3rd ed.; Butterworth-Heinemann: Oxford, UK.

Vedder, B. (2023), bldc. https://github.com/vedderb/bldc/ (Accessed on 05.09.2023)

Vempaty, S., He, Y., A Review of Car-Trailer Lateral Stability Control Approaches. SAE Technical Paper 2017-01-1580, 2017, https://doi.org/10.4271/2017-01-1580

ISSN: 2667-2812